Available online at www.sciencedirect.com
ScienceDirect
Trans. Nonferrous Met. Soc. China 24(2014) 2326−2330
Transactions of Nonferrous Metals Society of China
www.tnmsc.cn

Precipitation hardening behavior of dilute binary Al−Yb alloy

Chao-lan TANG[1], De-jing ZHOU[2]

1. College of Electromechanical Engineering, Guangdong University of Technology, Guangzhou 510006, China;
2. Scientific Research Institute, Yinbang Metal Clad Material Co., Ltd., Wuxi 214145, China

Received 17 October 2013; accepted 23 April 2014

Abstract: The precipitation hardening behavior in dilute Al−Yb alloys upon annealing at different temperatures was investigated to shed light on the mechanism of micro-alloying element in aluminum alloys. When aging at different temperatures, the samples showed their corresponding peak hardness in the range of 400−416 MPa due to the precipitation of Al_3Yb with L12 crystal structure. The coarsening kinetics of the Al_3Yb precipitates obeyed the LSW theory, which indicated that the coarsening process was controlled by the diffusion of Yb. The coherence between Al_3Yb particles and matrix was maintained until the particle size reached 11 nm. When the particle size increased to about 2 nm, the shearing mechanism started to change to Orowan mechanism.
Key words: aluminum alloy; microalloying; ytterbium; aging; coherency; precipitation hardening

1 Introduction

A continuing goal in aluminum alloy development is to improve the strength, ductility, thermal stability and weldability so as to obtain a good comprehensive performance. Intensive past research has been conducted, and it was found that coherent intermetallic precipitating, especially for the $L1_2$ structured intermetallic particle, is an effective approach for strengthening [1]. However, only a limited number of possibilities exist in Al-based alloys for the formation of coherent strengthening particles that are thermodynamically stable and have the ordered $L1_2$ structure [1,2]. Of the possibilities, additions of Sc, Er and Yb have been most commonly studied [2−4]. Extensive research has established that Al–Sc solid solution decomposes to form a fine dispersion of homogeneously nucleated, equilibrium precipitates of a stable $L1_2$ phase, Al3Sc, which can produce a significant age hardening [5]. Moreover, the Al3Sc dispersoids can stabilize the grain structure of the alloy and prevent recrystallization after hot rolling by pinning grain and subgrain boundaries [6,7]. Similar to Sc, the heavy rare-earth element Er exhibits an Al−Al3Er eutectic reaction with Al3Er exhibiting a stable $L1_2$ crystal structure [8]. DALEN et al [8] and WEN et al [9] had investigated the solubility of Er in aluminum and the isochronal aging behavior of Al−0.045(mole fraction, %)Er. LI et al [10] and NIE et al [11] carried out intensive research on the influence of Er on the microstructure and mechanical properties of commercial aluminum alloy and found that Er addition is capable of strengthening and nanoscale Al3Er dispersions can inhibit recrystallization. There are investigations on precipitation strengthening in Al−Zr−Yb alloys, which illustrates significant precipitation strengthening and thermal stability [4]. However, there is no systematic investigation on the precipitation hardening behavior of Al−Yb binary alloy. In this work, we will investigate the precipitation hardening behavior of an Al−0.3(%)Yb aged at temperatures of 250, 300, and 350 °C to shed light on the mechanism of micro-alloying element in aluminum alloys.

2 Experimental

An Al−0.3(mass fraction, %)Yb alloy was prepared by diluting commercially pure aluminum with an Al−30(mass fraction, %)Yb master alloy. Its chemical composition was verified using inductively coupled plasma-atomic emission spectroscopy. The melt was poured into an iron mold at about 720 °C to produce a

Foundation item: Project (2013AA031301) supported by Hi-tech Research and Development Program of China; Project (S2013ZR0611) supported by the National International Scientific and Technological Cooperation Program of China
Corresponding author: Chao-lan TANG; Tel: +86-20-13556120693; E-mail: tangchl@gdut.edu.cn
DOI: 10.1016/S1003-6326(14)63352-5

15 mm × 100 mm × 200 mm plate. Heat-treatments consisted of homogenization in air at 625 °C for 24 h, water quenching to room temperature, and aging in air at temperatures of 250, 300 and 350 °C for 5 min and 130 h, which was terminated by water quenching. Vickers microhardness was measured on polished samples using the average value from at least 10 independent measurements with a load of 1.96 N and a dwell time of 10 s. The common used unit of Vickers hardness is HV, but the unit is MPa in this work for comparing with other references [8,9]. The conversion of HV into MPa can use the equation HV_1=9.8 MPa. Slices for transmission electron microscopy (TEM) samples were cut from the plate, and were subsequently ground to less than 100 μm and punched into 3 mm discs. Thin foils for TEM observation were prepared by twin-jet polishing with an electrolyte solution consisting of 30% HNO_3 and 70% methanol below −30 °C. TEM observation was carried out by JEOL 2100 microscope with an operating voltage of 200 kV. The average precipitates radii, $\langle R(t)\rangle$, were measured from dark field images taken by the L12 superlattice reflections. To obtain statistically reliable data, more than 200 particles were analyzed on more than three micrographs for each aging condition.

3 Results and discussion

3.1 Age hardening behavior

The average hardness value of our specimens after homogenization and quenching but before aging is 240 MPa, which is higher than the hardness of about 180 MPa for pure Al [12], as expected from the presence of ytterbium in solid solution and primary Al_3Yb at the grain boundary. Figure 1 shows the TEM image of some typical primary Al_3Yb phases at the grain boundary and its corresponding selected area diffraction (SAD) pattern. It should be formed by divorced eutectic reaction as that of the primary Al_3Yb in Yb-containing alloys [13]. During solidification, supersaturated Yb atoms were expelled from the grain and accumulated at the front of the interface between solid and liquid. When Yb concentration approaches the eutectic point, Al_3Yb will form as part of the eutectic structure.

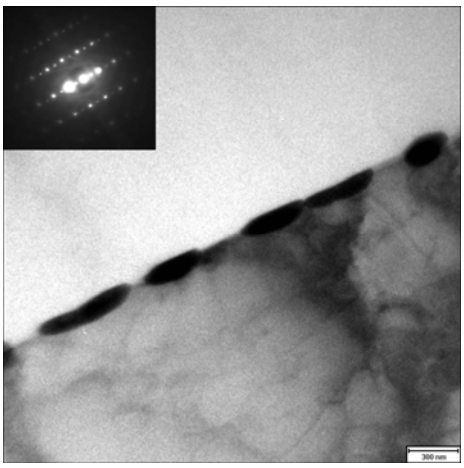

Fig. 1 TEM image of primary Al_3Yb phase and its corresponding SAD pattern

The homogenized alloy was aged at temperatures of 250, 300 and 350 °C, respectively. The microhardness as a function of the aging time is presented in Fig. 2. For a given aging temperature, with the increasing of the aging time, there is aging hardening behavior, which exhibits four different regions: 1) an incubation period; 2) a short transient period with a rapid increase in hardness values; 3) peak aging, a plateau at high hardness values; and 4) overaging, a decrease of the hardness [12]. The incubation period is very short, and the hardness increases immediately after aging treatment. The peak aging hardness values are similar to each other; however, the time taken to reach the maximum hardness decreases and the rate of hardness drop after peak aging increases as the aging temperature increases. The maximum hardness obtained is 415 MPa after aging at 250 °C for 1 h and this hardness level is retained for about 50 h. The maximum hardness of 350 °C aging is 400 MPa, which is obtained after aging for 5 min, and this hardness decreases quickly with overaging. This aging behavior is similar to that of the Al−Sc alloy, while the peak aging hardness is larger than that of the Al−Sc alloy with the same composition [12,14].

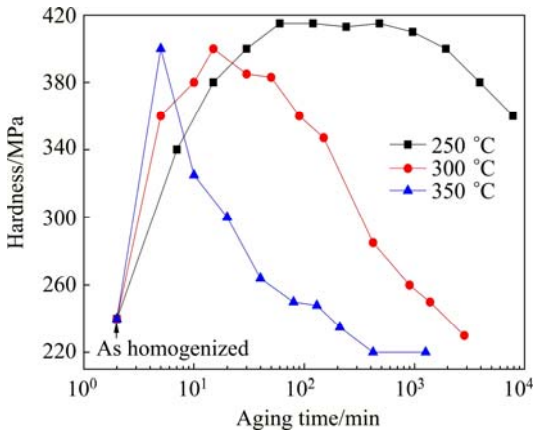

Fig. 2 Vickers microhardness as function of aging time at temperatures of 250, 300, 350 °C

The age hardening effect must be accommodated by precipitation of a secondary phase. From the Al−Yb equilibrium phase diagram, the supersaturated Al−Yb solid solution will decompose to form Al_3Yb phase [15]. TEM observations were carried out to investigate the hardening precipitates and four typical samples were selected to exhibit the precipitation characteristic. Figures 3(a) and (b) show the TEM micrographs of the

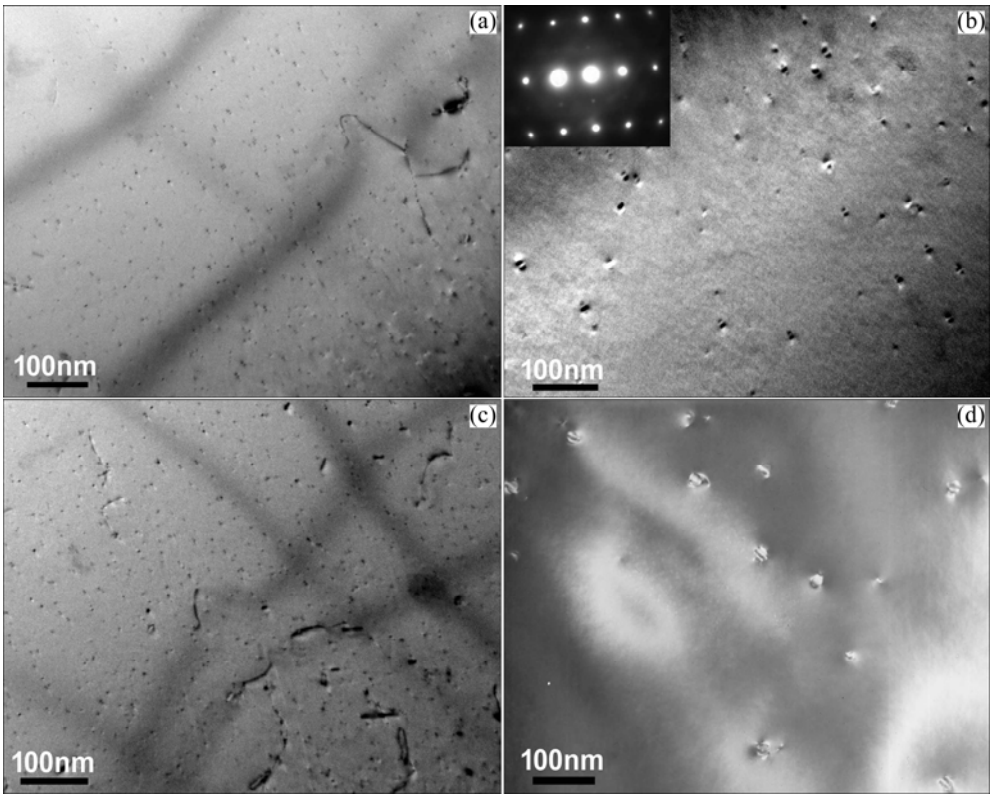

Fig. 3 TEM micrographs of samples aged at 250 °C for 1 h (a), aged at 250 °C for 130 h (b), aged at 300 °C for 15 min (c) and aged at 300 °C for 20 h (d)

sample annealed at 250 °C for 1 h and 130 h, respectively. A high number-density of nearly spherical precipitates was formed as a result of the aging treatment. These precipitates are Al_3Yb with L12 structure as indicated by the super-lattice diffraction point in the inserted SAD pattern. The precipitates are homogeneously distributed, which indicates that they are formed by continuous precipitation other than discontinuous precipitation such as precipitation of Al3Sc and Al3Zr in some Al−Sc [16] and Al−Zr [17] alloys. The average radii, $\langle R(t)\rangle$, of the precipitates are 1.5 and 5.0 nm in Figs. 3(a) and (b), respectively. The coffee-bean contrast pattern of the precipitates in Fig. 2(b) indicates that the precipitates are coherent with the Al matrix. Figures 3(c) and (d) show the TEM micrographs of the sample annealed at 300 °C for 15 min and 20 h, respectively. The average precipitate radii, $\langle R(t)\rangle$, of the precipitates are 2.5 and 10.5 nm, respectively. We can find that the precipitates with the average radius of 11 nm are semi-coherent with the matrix as indicated by the corresponding Ashby and Brown (AB) contrast as indicated in Fig. 3(d).

The transition from coherent to semi-coherent is controlled by the equilibrium between elastic energy and interfacial dislocation energy. With the increase of the precipitate radius, the elastic energy is so large as to break the coherent interface to form interfacial dislocation. The following relationship is valid for this transition at a critical radius, r_c [18,19]:

$$4\pi r_c^2\sigma=8\pi r_c^3 G\delta^2\frac{1+\nu}{3(1-\nu)} \tag{1}$$

where G and ν are the shear modulus and Poisson ratio of Al, respectively; δ is the lattice misfit between Al_3Yb and Al; σ is the interfacial dislocation energy per unit area, is related to d and can be expressed as follows [18,19]:

$$\sigma=\frac{Gb}{2\pi^2}\{1+\beta-(1+\beta)^{1/2}-\beta\ln[2\beta(1+\beta^2)^{1/2}-2\beta^2]\} \tag{2}$$

where b is the Burges vector and $\beta=\pi\delta/(1-\nu)$. Substitution of G=26.4 GPa, δ=0.037, b_{110}=0.286 nm and ν=0.34 in Eqs. (1) and (2) produces r_c=10.9 nm. The calculated value is very close to the measured one. It can be found that though the lattice misfit of Al_3Yb and Al (0.037) is much larger than that of Al_3Sc or Al (0.013), the r_c value (r_c=12.3 nm for Al3Sc [18]) has a minor difference because both of the elastic energy and interfacial misfit dislocation energy increase with the increase of the lattice misfit.

3.2 Coarsening kinetics of precipitates

To further investigate the coarsening kinetics of the precipitates, the change in the mean value of the precipitate radius, $\langle R(t)\rangle$, as a function of aging time is

measured at three different aging temperatures of 250, 300 and 350 °C. Figure 4 displays the increasing average precipitate radius, $\langle R(t)\rangle$, with increasing aging time at 250, 300 and 350 °C on a double logarithmic plot. For a given aging temperature, the $\langle R(t)\rangle$ vs aging time can be fitted with a line with a slope of approximately 1/3. This indicates that the kinetics of growth of Al_3Yb precipitate is consistent with the prediction of the LSW theory, a diffusion control Ostwald ripping theory firstly proposed by LIFSHITZ et al [20], as follows:

$$\langle R(t)\rangle^3 - \langle R(0)\rangle^3 = kt \quad (3)$$

where k is a constant representing the velocity of coarsening kinetics; $\langle R(0)\rangle$ is the average radius of the precipitates at the beginning of ripping. The intercept of the fitted line with the $\langle R(t)\rangle$ axis represents lg k (the logarithm of the velocity of coarsening kinetics, k). With increasing aging temperature, the increase of lg k values demonstrates an accelerating coarsening kinetics.

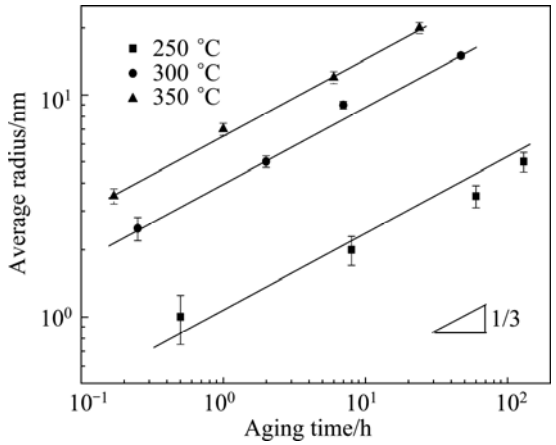

Fig. 4 Average precipitate radius, $\langle R(t)\rangle$, as function of aging time at temperatures of 250, 300 and 350 °C

3.3 Precipitation hardening mechanism

Combining the hardness values shown in Fig. 2 and the results of precipitate coarsening during aging shown in Fig.4, Fig. 5 shows the increase in hardness due to Al_3Yb precipitation as a function of precipitate radius. The similarity of the maximum hardness of different aging temperatures implies that the volume fraction of Al_3Yb is approximately constant, so direct comparison between data points in Fig. 5 is reasonable [12]. There is a maximum in hardness for radii between 1.5 and 2.0 nm, then the hardness decreases with increasing radius. This result indicates a transition from a dislocation shearing mechanism to an Orowan bypass mechanism as observed in Al−Sc alloy [12]. We can find that the maximum hardness is larger than that of the Al−Sc alloy with the same composition [12,14]. This indicates that strengthening effect of Al_3Yb is larger than that of Al3Sc as the shearing mechanism is effective. The shearing stress is the highest among the order strengthening and the sum of coherency and modulus mismatch strengthening. There are no available data of anti-phase boundary (APB) energy and modulus of Al_3Yb, so we cannot give a definitely description of the strengthening. One thing that can be determined is that the coherency strengthening effect of Al_3Yb is larger than that of Al3Sc due to the larger lattice mismatch with the Al matrix.

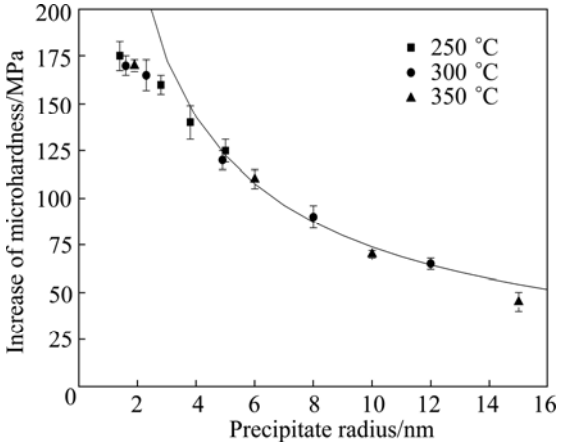

Fig. 5 Increase in microhardness versus precipitate radius for alloy aged at different temperatures

The hardness−radius relationship with radius larger than 2 nm is fitted by an Orowan mechanism as follows [1, 12]:

$$\Delta\sigma_{\mathrm{Or}} = M\frac{0.4Gb}{\pi\sqrt{1-\nu}}\frac{\ln\left(\frac{2r}{b}\right)}{\left[\left(\frac{3\pi}{4f}\right)^{1/2}-1.64\right]r} \quad (4)$$

where $r=\pi\langle R(t)\rangle/4$, is the mean planar precipitate radius [1]; M=3.06 is the mean matrix orientation factor for Al [1,12]; f is the volume fraction of Al_3Yb precipitates; b, G and ν have the same values as those in Eq. (1). The hardness can be fitted by Eq. (4) with f=0.1% for radius within the range of 2−10 nm, using a conversion factor of 3 between hardness and strength.

4 Conclusions

1) Heat treatment resulted in L12 Al_3Yb precipitates which is coherent with radius less than 11 nm while semicohenrent with radius larger than 11 nm.

2) The coarsening kinetics of L12 Al_3Yb precipitates is controlled by diffusion and obeys the LSW theory.

3) The precipitates strengthen the Al matrix as indicated by the aging hardening curves. The maximum hardness obtained is 415 MPa after aging at 250 °C for

1 h. The peak aging hardness values are similar to each other; however, the time taken to reach the maximum hardness decreases and the rate of hardness drop after peak aging increases as the aging temperature increases.

4) The strength is controlled by dislocation shearing mechanism for precipitate with radius less than 2 nm, and the Orowan dislocation bypass mechanism for larger precipitates.

References

[1] KNIPLING K E, DUNAND D C, SEIDMAN D N. Criteria for developing castable, creep-resistant aluminium-based alloys — A review [J]. Zeitschrift fur Metallkunde, 2006, 97: 246−265.

[2] ROGAL L, DUTKIEWICZ J, ATKINSON H V, LITYNSKA-DOBRZYNSKA L, CZEPPE T, MODIGELL M. Characterization of semi-solid processing of aluminium alloy 7075 with Sc and Zr additions [J]. Materials Science and Engineering A, 2013, 580: 362−373.

[3] WATTANACHAI P, NAKORN S, CHAOWALIT L. Influence of Sc modification on the fluidity of an A356 aluminum alloy [J]. Journal of Alloys and Compounds, 2013, 487: 453−457.

[4] ZHANG Y Z, ZHOU W, GAO H Y, HAN Y F, WANG K, WANF J, SUN B D, GU S W, YOU W R. Precipitation evolution of Al−Zr−Yb alloys during isochronal aging [J]. Scripta Materialia, 2013, 69: 477−480.

[5] FILATOV Y A, YELAGIN V I, ZAKAHROV V V. New Al−Mg−Sc alloys [J]. Materials Science and Engineering A, 2000, 280: 97−101.

[6] ROBSON J D. A new model for prediction of dispersoid precipitation in aluminium alloys containing zirconium and scandium [J]. Acta Materialia, 2004, 52: 1409−1421.

[7] RIDDLW Y W, SANDERS T H. Recrystallization performance of AA7050 varied with Sc and Zr [J]. Material Science Forum, 2000, 331−337: 780−799.

[8] van DALEN M E, KARNESKY R A, CABOTAJE J R, DUNAND D C, SEIDMAN D N. Erbium and ytterbium solubilities and diffusivities in aluminum as determined by nanoscale characterization of precipitates [J]. Acta Matererialia, 2009, 57: 4081−4089.

[9] WEN S P, GAO K Y, LI Y, HUANG H, NIE Z R. Synergetic effect of Er and Zr on the precipitation hardening of Al−Er−Zr alloy [J]. Scripta Materialia, 2011, 65: 592−595.

[10] LI Yan, WEN Shen-ping, GAO Kun-yuan, HUANG Hui, NIE Zuo-ren. Precipitation evolution in Al−Er−Zr alloys [J]. The Chinese Journal of Nonferrous Metals, 2011, 23(2): 336−342. (in Chinese)

[11] NIE Zuo-ren, WEN Shen-ping, HUANG Hui, LI Bo-long, ZUO Tie-yong. Research progress of Er-containing aluminium alloy [J]. The Chinese Journal of Nonferrous Metals, 2011, 21(10): 2361−2370. (in Chinese)

[12] SEIDMAN D N, MARQUIS E A, DUNAND D C. Precipitation strengthening at ambient and elevated temperatures of heat-treatable Al(Sc) alloys [J]. Acta Materialia, 2002, 50: 4021−4035.

[13] WEN S P, XING Z B, HUANG H, LI B L, WANG W, NIE Z R. The effect of erbium on the microstructure and mechanical properties of Al−Mg−Mn−Zr alloy [J]. Materials Science and Engineering A, 2009, 516: 42−49.

[14] van DALEN M E, DUNAND D C, SEIDMAN D N. Effects of Ti additions on the nanostructure and creep properties of precipitation-strengthened Al−Sc alloys [J]. Acta Materialia, 2005, 53: 4225−4235.

[15] MONDOLFO L F. Aluminum alloys: Structure and properties [M]. Boston: Butterworths, 1976.

[16] NORMAN A F, PRANGNELL P B, MCEWEN R S. The solidification behaviour of dilute aluminium−scandium alloys [J]. Acta Materialia, 1998, 46: 5715−5732.

[17] RYUM N. Precipitation and recrystallization in an A1−0.5wt.% Zr-alloy [J]. Acta Metallurgica, 1969, 17: 269−278.

[18] IWAMURA S, MIURS Y. Loss in coherency and coarsening behavior of Al3Sc precipitates [J]. Acta Materialia, 2004, 52: 591−600.

[19] JESSER W A. On the theory of loss of coherency by spherical precipitates [J]. Philosophical Magazine, 1968, 19: 993−999.

[20] NOVOYNY G M, ARDELL A J. Precipitation of Al3Sc in binary Al Sc alloys [J]. Materials Science and Engineering A, 2001, 318: 144−154.

Al−Yb 合金的析出强化行为

唐超兰[1]，周德敬[2]

1. 广东工业大学 机电工程学院，广州 510006；

2. 无锡银邦金属复合材料有限公司研究院，无锡 214145

摘　要：研究了稀二元 Al−Yb 合金在不同时效温度下的析出强化行为。结果表明，在时效过程中析出了细小、弥散的 L12 结构 Al_3Yb 相，时效析出所能达到的峰值硬度为 400~416 MPa，各温度的峰值硬度比较接近。L12 结构的 Al_3Yb 析出相的粗化动力学遵循 LSW 理论，表明粗化由溶质原子扩散控制。当 Al_3Yb 析出相的半径小于 11 nm 时其与基体保持共格关系，大于 11 nm 时开始出现半共格现象。当析出相的半径小于 2 nm 时，时效强化的机理是位错切割机制，大于 2 nm 时则主要为位错绕过的 Orowan 机制。

关键词：铝合金；微合金化；镱；时效；共格；析出强化

(Edited by Hua YANG)